Composite Structures 184 (2018) 894–903

Contents lists available at ScienceDirect

Composite Structures

journal homepage: www.elsevier.com/locate/compstruct

Simultaneous ply-order, ply-number and ply-drop optimization of laminate wind turbine blades using the inverse finite element method

Alejandro Albanesi[a,*], Facundo Bre[a], Victor Fachinotti[a], Cristian Gebhardt[b]

[a] CIMEC Centro de Investigación de Métodos Computacionales, UNL, CONICET, Col. Ruta 168 s/n, Predio Conicet Dr Alberto Cassano, 3000 Santa Fe, Argentina
[b] Institut für Statik und Dynamik, Leibniz Universität Hannover, Appelstraße 9A, 30167 Hannover, Germany

ARTICLE INFO

Keywords:
Wind turbine blade
Optimization
Composite materials
Inverse finite element
Multilayered shells

ABSTRACT

This paper presents a novel methodology to simultaneously determine the optimal ply-order, ply-number and ply-drop configuration of laminate wind turbine blades using simulation-based optimization, considering the shape that the laminates are expected to attain after large elastic deformations. This methodology combines Genetic Algorithms with the Inverse Finite Element Method.

As an actual engineering application, we redesigned the composite stacking layout of a medium-power 40-kW wind turbine blade to reduce its weight, subjected to mechanical and manufacturing constraints such as allowable tip deflection, maximum stress, natural frequencies, and maximum number of successive identical plies. Results demonstrate weight reductions of up to 15% compared to the initial layout, proving that the proposed methodology is a robust redesign tool capable of effectively determining the optimal composite stacking layout of laminate wind turbine blades.

1. Introduction

In the pursuit of better, more competitive and more efficient wind turbines, the structural layout of the blades is one of the design aspects that can lead to significant reductions of weight and costs, while maintaining the reliability of the machine. Improvements on the stacking sequence and the number of plies along the blade provide not only weight and costs savings in the rotor, but also in the tower and foundation. The use of composite materials in the manufacturing process of the blades is a natural choice due to many technical and economic reasons, such as outstanding mechanical properties, excellent strength-to-weight ratio, availability, reliability, and competitive cost. The vast amount of scientific works addressing the search of the optimal stacking sequence and number of plies in the composite laminates of the blades proves that this is one of the most popular design problems in the wind energy community.

The use of laminates with variable stiffness along the blade [1] is of particular interest due to their superior structural performance compared to laminates with longitudinally constant stiffness [2]. Variable stiffness laminates taper material distribution that is achieved by *ply drop*: A material layer can be dropped from the root to the tip of the blade, if it is not essential for its structural stability.

Hence, the optimal design of a blade can be determined by finding the proper laminate distribution that minimizes the weight of the blade, while satisfying all given constraints [3]. This is usually a nonlinear programming problem with integer design variables, like the number of plies and their order, which are continuous design variables, where the mechanical constraints (minimal compliance, maximal stress) are determined using computational mechanics.

Genetic algorithms (GA) [4], based on the natural principle of "survival of the fittest", are by far the widest methods for the solution of this kind of problem. In a pioneering work on optimization of tapered laminates, Kim et al. [5] developed the "patch-wise layout design method" using GA for minimizing the weight of the structure subject to a strength constraint based on the Tsai-Hill fail criterion, considering as design variables the ply angles and the number of plies in each patch. To ensure fiber continuity between patches, only the stacking sequence in the patch with the maximum number of plies is optimized, and the same sequence is adopted for the remaining patches (although plies can be dropped from patches where the failure constraint is satisfied). Irisarri et al. [6] used a Pareto-based GA to minimize the mass and maximize the buckling margin for a tapered laminate, subject to strength constraint for avoiding instability issues throughout the structure (even if the buckling margin is maximized, it could remain low). They used a Stacking Sequence Table (SST) to describe the sequence of ply-drops ensuring the transition between patches, which allowed them to satisfy design rules without additional constraints. Fan et al. [7] minimized a unique function defined as the sum of the weight

* Corresponding author.
E-mail address: aalbanesi@cimec.santafe-conicet.gov.ar (A. Albanesi).

http://dx.doi.org/10.1016/j.compstruct.2017.10.051
Received 29 May 2017; Received in revised form 4 September 2017; Accepted 16 October 2017

of the laminate and a term that decreases as the buckling margin increases, penalized by factors considering contiguity and disorientation. They introduced the ply-composition and the ply-ranking chromosomes, whose construction forced the satisfaction of the design rules on continuity, balance and symmetry without using constraints.

Specific to wind turbine applications, Dal Monte et al. [8] presented a multi-objective GA optimization procedure to minimize the mass and maximum displacement of a 7.22-meter blade for the AOC 15/50 Horizontal Axis Wind Turbine (HAWT), by changing the material layup and placement in the shell skin. Integer design variables to optimize categorical variables are used in this case. In a more recent work, Dal Monte et al. [9] present a coupled optimization procedure where both aerodynamic and structural parameters are considered as the design variables, to improve the performance and mechanical integrity of the AOC 15/50 HAWT. In this approach, the blade element momentum (BEM) and the finite element method (FEM) are used for the aerodynamic and structural response, respectively, and the optimization is carried out by GA. Wang et al. [10] applied GA to minimize the weight of a blade of a 30-kW Vertical Axis Wind Turbine (VAWT), subject to constraints on stress, deformation, vibration and buckling, manufacturing and continuity. They consider not only integer design variables (the number of unidirectional plies at each region of the blade) but also continuous ones (the location of spar caps and the thickness of shear webs). Fagan et al. [11] minimized the weight, penalized by the deformation excess, of a 13-meter blade for a medium-power HAWT. In this case, they considered integer design variables defining the amount of plies in the shell skin, the shear webs, and the spar caps of the blade, the end point of the core in the shear webs and the number of shear webs.

In a previous work [12], we widely describe the use of the Inverse Finite Element Method (IFEM) for the design of the blade of a 40 k three-blade HAWT. In this work, we introduce a new method for the determination of the optimal number and order of plies in tapered laminates, capable of accounting for the shape the laminates are expected to attain after large elastic deformations. As usual in the above mentioned literature, we use GA to minimize the weight of the structure subject to manufacturing and mechanical constraints, the latter being evaluated by numerical structural solver. Here, we make a crucial contribution to the optimization of slender structures undergoing large elastic deformations (like most of the turbine blades): the use of IFEM [12,13] for structural analysis. IFEM computes the manufacturing shape of a structure such that it attains a prescribed shape under given loads. By this way, a major requirement is taken into account in the optimal design of the blade: It has to attain a given aerodynamically efficient shape when it is largely deformed by the service loads. This is a novel methodology, and to the best of the authors' knowledge, no other combination of an optimization method and IFEM has been reported in literature so far. Hence, the former blade of [12] is taken as the base case to highlight the current optimization results.

This paper is organized as follows: Section 2 presents the design problem under study, and describes the geometry and material layout of the reference blade, and the mechanical properties of the composite materials adopted. Section 2.3 describes the objective function, the design variables, and the design constraints of the optimization problem. Section 3 describes the GA algorithm used in this work, and its specific setup. Numerical results are given in Section 4, and the concluding remarks in Section 5.

2. Case study

In order to validate the current optimization methodology, let us take as reference the blade of a 40 kW three-blade HAWT designed in our previous work [12]. This turbine has a radius of $R = 6.70$ m and, under operating conditions, it rotates at 72 RPM for a wind velocity of 7 m/s. Three airfoils from the SG604X family [14] were selected for the root (SG6040), the mid-span (SG6042) and the tip of the blade (SG6043), while intermediate airfoils were defined by linear interpolation. The adimmensional chord length and the twist angle distribution vary along the span following classical Schmitz theory. Both of these values are presented in Table 1 along the adimmensional blade span. The resulting shape of the blade is shown in Fig. 1.

Table 1
Chord length and twist angle distribution along the adimmensional blade span.

Blade span [r/R]	Chord [c/R]	Twist [degrees]
0.12	0.170	28.51
0.19	0.140	19.08
0.27	0.118	13.49
0.35	0.090	9.95
0.42	0.080	7.59
0.50	0.070	5.93
0.58	0.060	4.72
0.65	0.055	4.12
0.73	0.050	3.72
0.81	0.045	3.43
0.88	0.041	3.31
0.96	0.039	3.25
1.00	0.038	3.25

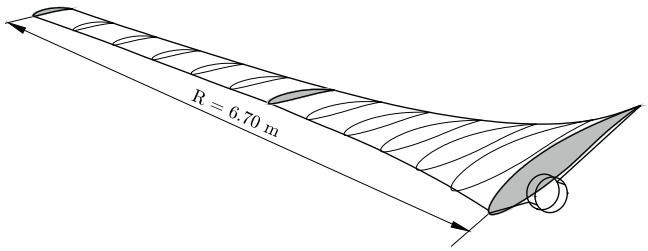

Fig. 1. Geometry of the reference blade, determined in [12].

The aerodynamic pressure over the reference blade was computed using Computational Fluid Dynamics (CFD) for the given operating conditions in [12], and it is depicted in Fig. 2. This problem was numerically solved using the finite volume method as implemented into the open-source software OpenFoam. The steady-state solver for incompressible and turbulent flow *simpleFoam* with the k-ω turbulence model was used along with the multiple reference frame approach

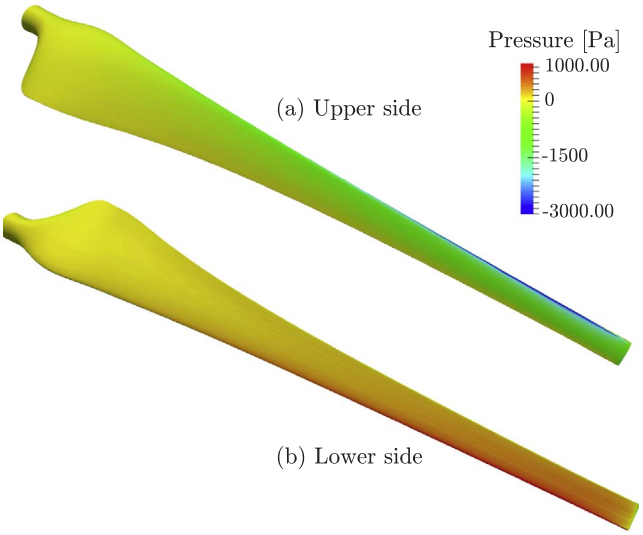

Fig. 2. Resultant aerodynamic pressure over the blade, computed in [12]. View from the upper side (a) and from the lower side (b).

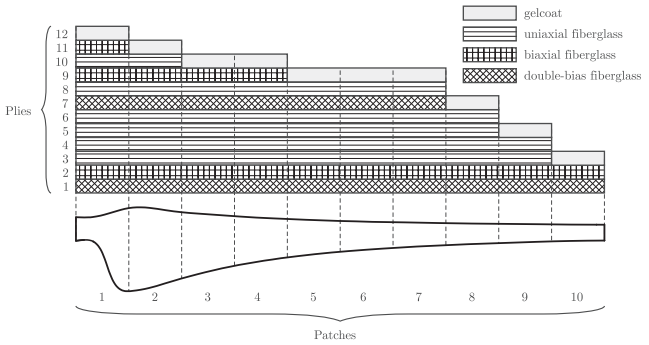

Fig. 3. Layout of the reference blade.

trough the *fvOptions*. The boundary conditions are prescribed wind velocity at the inlet, and uniform atmospheric pressure in the lateral surface (open boundary) and in the outlet boundary, and the surface of the blades is assumed to be a smooth no-slip wall. This procedure was validated in [12]. The resultant aerodynamic forces are determined by these pressure gradients in combination with the viscous flow.

The blade was assumed to be made of a tapered laminate of multiple plies of double-bias, biaxial and uniaxial fiberglass, and epoxy gelcoat, as shown in Fig. 3. The fiberglass consists of an epoxy resin reinforced by E-type glass fibers with volume fraction of 60%. Fibers in the plies of uniaxial fiberglass are parallel to the longitudinal axis of the blade, while they are either parallel or normal to this axis in the plies of biaxial fiberglass, and they are inclined ± 45° with respect to this axis in the plies of double-bias fiberglass. In all cases, ply 1 always denotes the layer next to the core of the blade, the outer ply is made of epoxy gelcoat, and the stacking sequence is repeated at the lower and upper side (i.e., it is symmetric with respect to the core of the blade). The design of this reference blade was inspired by similar designs of Sandia [15] and NREL [16]. Material properties are listed in Table 2.

The material distribution throughout the blade in combination with the angular velocity, determines the stationary inertial loads. These body forces, together with the resultant aerodynamic forces, have as resultant the service loads producing the large elastic deformation of the blade.

2.1. Finite element mesh

The structured quadrilateral mesh used for the IFEM structural analysis is depicted in Fig. 4, and consists of 22,000 elements, 22,044 nodes, and 110,220 degrees of freedom (see [12]). It was created using the open source meshing software GMSH [17]. A mesh sensitivity analysis was performed with meshes of 6000, 12,000, 22,000, 26,000, and 32,000 elements. Results showed that the 22,000 elements mesh was the best compromise between accuracy and computational cost.

Table 2
Mechanical properties of the materials in the blade.

Property	Uniaxial	Biaxial	Double bias	Gelcoat
Longitudinal elastic modulus E_X [GPa]	44	44	44	5
Transverse elastic modulus E_Y [GPa]	12.6	44	44	5
Shear modulus G_{XY} [GPa]	10	35	15	1.8
Density [Kg/m^3]	1117	1004	914	650
Poisson ratio	0.32	0.36	0.36	0.4
Thickness [mm]	0.50	0.50	0.35	0.25
Long. tensile strength X_T [MPa]	1020	1020	850	–
Long. compressive strength X_C [MPa]	610	610	550	–
Transverse tensile strength Y_T [MPa]	41	1020	850	–
Transverse compressive strength Y_C [MPa]	140	610	550	–
Shear strength S [MPa]	72	95	76	–

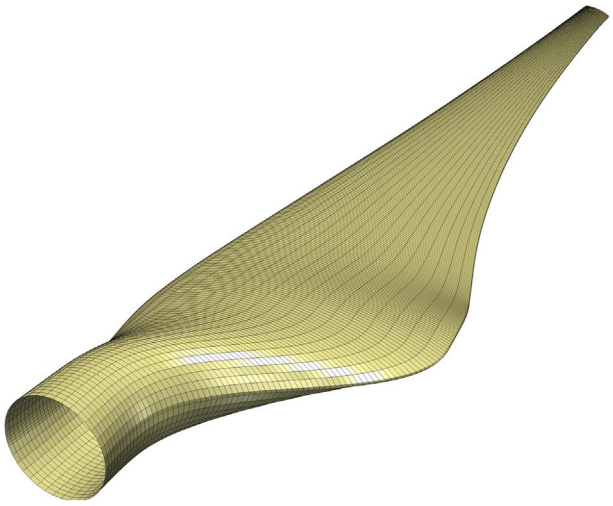

Fig. 4. Quadrilateral finite element mesh. Represents the desired shape of the blade after deformation.

2.2. Description of the IFEM structural solver

To ensure the deformed blade attains its efficient aerodynamic shape (that given by Fig. 1), we used the model of Albanesi et al. [12], based on the IFEM for shells developed by Fachinotti et al. [13]. The analysis domain consists in the geometry of the blade after large elastic deformations, caused by given service loads. This deformed shape of the blade is that determined to be efficient using an aerodynamics analysis methods. From this analysis, the aerodynamic loads on the blade are known. Then, multilayer composite materials need to be chosen to manufacture the blade, and after this selection, the stationary inertial loads on the blade are known. With this information, IFEM is used to compute the manufacturing shape of the blade, solving a nonlinear equilibrium equation only once. This is a one-step, one-direction strategy where the aerodynamics analysis feeds the structural analysis, and no further interaction between both solvers is required, see Fig. 5.

Our IFEM model is the inverse counterpart of the widely known MITC4 shell element [18], a formulation based on the degenerated solid approach in which governing equations are the same as those for general solids, and in the Mindlin-Reissner shell theory in which transverse shear deformation is considered, and henceforth are capable of representing thin to moderately thick shells with multiple layers of transversely orthotropic materials. This section presents a very brief description of this IFEM model, and the interested reader is encouraged to visit references [13,12] for further details and validation benchmarks.

2.2.1. Finite element technology

Let us consider the undeformed configuration $\mathscr{B}^0$, and deformed configuration $\mathscr{B}$, depicted in Fig. 6. The position of any point $\boldsymbol{X}$ in $\mathscr{B}^0$ is expressed as follows:

$$\boldsymbol{X}(\xi_1,\xi_2,\xi_3) = \overline{\boldsymbol{X}}(\xi_1,\xi_2) + \xi_3\frac{H}{2}\boldsymbol{T}(\xi_1,\xi_2), \tag{1}$$

where $\overline{\boldsymbol{X}}$ lies in the midsurface $\mathscr{S}^0$ of $\mathscr{B}^0$,$\boldsymbol{T}$ is the material director vector, H is the thickness, and $\{\xi_1,\xi_2,\xi_3\}$ is a system of natural coordinates with origin $\overline{\boldsymbol{X}}$, so that ξ_1 and ξ_2 lie in $\mathscr{S}^0$. After deformation, the point $\boldsymbol{X} \in \mathscr{B}^0$ occupies the position $\boldsymbol{x} \in \mathscr{B}$ in $\mathscr{B}$ with midsurface $\mathscr{S}$:

$$\boldsymbol{x}(\xi_1,\xi_2,\xi_3) = \overline{\boldsymbol{x}}(\xi_1,\xi_2) + \xi_3\frac{h}{2}\boldsymbol{t}(\xi_1,\xi_2), \tag{2}$$

where $\overline{\boldsymbol{x}} \in \mathscr{S}$,$\boldsymbol{t}$ is the unit vector known as spatial director, and $h = h(\xi_1,\xi_2)$ is the thickness of the deformed shell. Since the Mindlin-

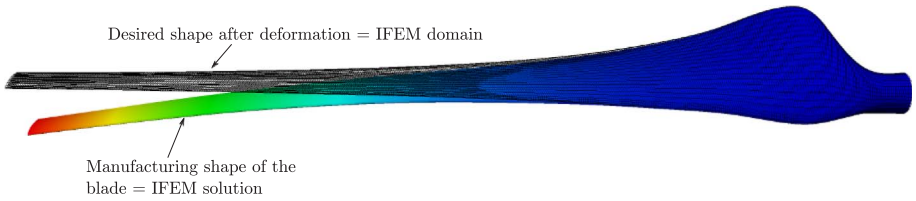

Fig. 5. Inverse analysis of wind turbine blades: The efficient aerodynamic shape of the blade, depicted in wireframe, is the domain of IFEM. The manufacturing shape of the blade, depicted in color gradient, is the IFEM solution.

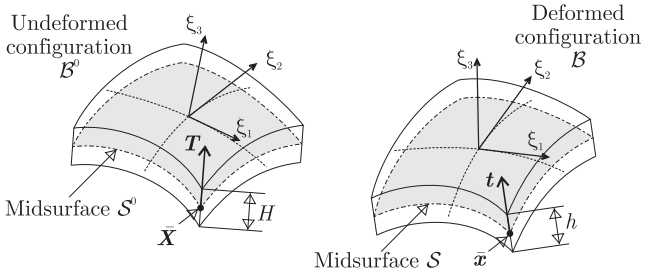

Fig. 6. Undeformed and deformed configurations of a shell.

Reissner plate theory is adopted, $\boldsymbol{t}$ does not have to be normal to $\mathscr{S}$, if $\boldsymbol{T}$ is normal to $\mathscr{S}^0$ (and vice versa) as an effect of shear deformation, and assumes that the strain normal to the midsurface is null, so $h = H$.

As in standard isoparametric finite element formulations, $\boldsymbol{x} \in \mathscr{B}$ and $\boldsymbol{X} \in \mathscr{B}^0$ are interpolated as:

$$\boldsymbol{X}(\xi_1,\xi_2,\xi_3) = \varphi_i\left[\overline{\boldsymbol{X}}_i + \frac{\xi_3}{2}h\boldsymbol{T}_i\right] = \boldsymbol{\Phi}(\xi_1,\xi_2,\xi_3)\boldsymbol{Q}, \tag{3}$$

$$\boldsymbol{x}(\xi_1,\xi_2,\xi_3) = \varphi_i\left[\overline{\boldsymbol{x}}_i + \frac{\xi_3}{2}h\boldsymbol{t}_i\right] = \boldsymbol{\Phi}(\xi_1,\xi_2,\xi_3)\boldsymbol{q}, \tag{4}$$

with

$$\boldsymbol{\Phi} = \left[\varphi_1\boldsymbol{I} \;\; \tfrac{\xi_3}{2}h\varphi_1\boldsymbol{I} \;\; \cdots \;\; \varphi_N\boldsymbol{I} \;\; \tfrac{\xi_3}{2}h\varphi_N\boldsymbol{I}\right], \tag{5}$$

$$\boldsymbol{Q} = \begin{bmatrix} \overline{\boldsymbol{X}}_1 \\ \boldsymbol{T}_1 \\ \vdots \\ \overline{\boldsymbol{X}}_N \\ \boldsymbol{T}_N \end{bmatrix}, \qquad \boldsymbol{q} = \boldsymbol{Q} = \begin{bmatrix} \overline{\boldsymbol{x}}_1 \\ \boldsymbol{t}_1 \\ \vdots \\ \overline{\boldsymbol{x}}_N \\ \boldsymbol{t}_N \end{bmatrix}, \tag{6}$$

where $(\overline{\boldsymbol{X}}_i,\boldsymbol{T}_i)$ defines the position of the node $i = 1,2,...N$ of the undeformed finite element, $(\overline{\boldsymbol{x}}_i,\boldsymbol{t}_i)$ defines the position of the node i of the deformed finite element, and $\varphi_i = \varphi_i(\xi_1,\xi_2)$ is the 2-D shape function associated with node i;I is the 3×3 identity matrix. The deformation of the shell is measured using the Green–Lagrange strain tensor defined as

$$E = \underbrace{\frac{1}{2}(g_\alpha\cdot g_\beta - G_\alpha\cdot G_\beta)}_{E^{\text{cov}}_{\alpha\beta}} G^\alpha \otimes G^\beta, \tag{7}$$

where

$$g_\alpha = \partial x/\partial\xi_\alpha, \qquad G_\alpha = \partial X/\partial\xi_\alpha, \qquad [G^1|G^2|G^3] = [G_1|G_2|G_3]^{-T} \tag{8}$$

To avoid shear locking, we use the MITC4 formulation, initially proposed by Dvorkin and Bathe [18]. The MITC4 finite element is a quadrangle with nodes located at its vertices, and bilinear shape functions ϕ_i. Inside this element, the covariant strain fields E^{cov}_{ij} are defined by Eq. (7), except the fields E^{cov}_{13} and E^{cov}_{23} that are replaced by "assumed" strain fields.

The equilibrium of degenerated solid shell models is governed by the same variational principle governing the equilibrium of general solids for all admissible variations of the displacement u:

$$\int_{\mathscr{B}^0} S^{\alpha\beta}\delta E_{\alpha\beta}\,\mathrm{d}V = \mathscr{W}^{\text{ext}}(\delta u). \tag{9}$$

Eq. (9) can be transformed into

$$\int_{\mathscr{B}^0} S^{\alpha\beta}\delta E_{\alpha\beta}\,\mathrm{d}V = \delta q^T F^{\text{int}}(q,Q), \tag{10}$$

where $F^{\text{int}}(q,Q)$ is the vector of nodal internal loads. Assuming the external loads to be lumped at the nodes and grouped in the vector of nodal external forces F^{ext}, the r.h.s. of Eq. (9) can be written as

$$\mathscr{W}^{\text{ext}}(q,Q) = \delta q^T F^{\text{ext}}(q,Q), \tag{11}$$

where it is admitted that the external forces generally depend on Q (body forces are usually given by unit undeformed volume) and q (as in the case of wind pressure).

Following Simo et al. [19], the increment of the director vector t_i is computed as $\delta t_i = \widetilde{\lambda}_i\delta\widetilde{t}_i$, where $\delta\widetilde{t}_i$ is a vector lying in the plane $\{i,j\}$ of the fixed global Cartesian frame $\{i,j,k\}$, and $\widetilde{\lambda}_i$ is the 3×2 matrix made of the first two columns of the orthogonal transformation matrix $\boldsymbol{\lambda}_i$ that maps the director vector update from $\delta t_i \in \mathbb{R}^3$ to $\delta\widetilde{t}_i \in \mathbb{R}^2$ (see [13] for details). Thus, the nodal director update involves only two degrees of freedom, making the current formulation have five degrees of freedom per node.

Finally, the following nonlinear equilibrium equation for direct FEM degenerated-solid shells is obtained:

$$R(q,Q) = F^{\text{int}}(q,Q) - F^{\text{ext}}(q,Q) = 0. \tag{12}$$

In IFEM, the loaded configuration $\mathscr{B}$ as well as the external loads, responsible for deforming the shell from $\mathscr{B}^0$ to $\mathscr{B}$, are assumed to be known. Since $\mathscr{B}$ is the known domain, at each shell finite element the vector of nodal internal loads F^{int} can be written as $\int_{\mathscr{B}^0} F\,\mathrm{d}V = \int_{\mathscr{B}} f\,\mathrm{d}v$, with $f = FJ^{-1}$, where J is the Jacobian determinant of the transformation from $\mathscr{B}^0$ to $\mathscr{B}$

$$J = \frac{\mathrm{d}v}{\mathrm{d}V} = \frac{(x_1 \times x_2)\cdot x_3}{(X_1 \times X_2)\cdot X_3}. \tag{13}$$

At this point, we make use of the close relationship between FEM and IFEM: Both have the identical governing equation that is given by the discrete equilibrium Eq. (12), differing only in the fact that knowns and unknowns are interchanged. Then, Eq. (12) defines also the equilibrium equation for IFEM applied to degenerated solid shells, being now a nonlinear equation for the unknown Q for a given q. This is a nonlinear equation to be solved using the Newton–Raphson method: At the iteration $k + 1$,Q is updated by solving the linear equation for δQ:

$$R(q,Q^{(k+1)}) = R(q,Q^{(k)}) + \left.\frac{\partial R}{\partial Q}\right|_{Q^{(k)}} \Delta Q = 0, \tag{14}$$

where $\partial R/\partial Q$ is the tangent stiffness matrix (see [13] for details).

The IFEM solution must pass a series of topological, mechanical, and numerical tests that assure its feasibility. These tests consist in: (*i*) a topological test for detecting inter-penetrated elements, (*ii*) a mechanical test to verify the validity of the hypothesis of elasticity, and (*iii*) a numerical test to verify the uniqueness of the solution (including a test for unstable equilibrium states such as buckling phenomena). If these tests are successful, the IFEM solution will attain the desired prescribed shape when it is subjected to service loads, and buckling is not encountered during deformation. If any of the tests fail, the IFEM output is an infeasible solution and should not be considered. Further details on these tests can be found in [12,13,20,21].

The IFEM model has been implemented in the open source software

GNU Octave 4.0.3 [22], built with and ad hoc configuration that includes several high performance libraries such as OpenBlas 0.2.19, Suisparse 4.5.4, ARPACK-NG 3.5.0, and LLVM-3.4 for the use of the JIT (just in time) compiler implementation for large loops.

2.3. Optimization of the blade

To optimize the blade, we mean to solve the following optimization problem:

$$\min_{x\in\mathscr{X}} w(x), \tag{15}$$

where w is the weight of the blade, and x is the set of design variables defining the ply layout based on the admissible design space $\mathscr{X}$.

The turbine blade is assumed to be divided into 10 patches as shown in Fig. 3, and ply drops are allowed between patches. Following Ghiasi et al. [1], in this work we consider a patch to be a region within the structure where the lamination sequence is uniform. Like in the reference blade, besides the outer ply that is always made of gelcoat, a maximum of 11 stacked plies is allowed. A priori, all the plies are assumed to start at the root of the blade, although some of them could be dropped from the beginning (i.e., these plies do not exist). Now, let us characterize any particular layout by the following vector of design variables:

$$x = [m_1 \quad m_2 \quad \dots \quad m_{11} \quad | \quad d_1 \quad d_2 \quad \dots \quad d_{11} \quad] \tag{16}$$

where m_i and d_i denote the material and the end patch of the ply i. Both variables are integer, with $1 \leqslant d_i \leq 10$ and

$$m_i = \begin{cases} 0 & \text{empty ply,} \\ 1 & \text{uniaxial fiberglass,} \\ 2 & \text{biaxial fiberglass,} \\ 3 & \text{double-bias fiberglass.} \end{cases} \tag{17}$$

If $m_i = 0$, the ply i is assumed to have zero thickness, i.e., it does not exist, and d_i becomes irrelevant. Considering such empty ply allows to control the number of plies in the laminate.

So, the vector of design variables characterizing the reference blade shown in Fig. 3 is

$$x_{\text{ref}} = [3 \quad 2 \quad 1 \quad 1 \quad 1 \quad 1 \quad 3 \quad 1 \quad 2 \quad 1 \quad 2 \quad | \quad 10 \quad 10 \quad 9 \quad 9 \quad 8 \quad 8 \quad 7 \quad 7 \quad 4 \quad 2 \quad 1].$$

Note that such parameterization automatically ensures fiber continuity: The ply with $m_i > 1$ starts at the root and is dropped at the end of patch p_i. Further, by considering such x as design variables of the optimization problem (15), we are simultaneously optimizing the ply order (given by $m_1,m_2,\dots$excluding those empty plies having $m_i = 0$), the ply number (equal to the maximum number of plies minus the number of empty plies) and ply drops (determined by d_i).

2.3.1. Constraints

The solution of the optimization problem (15) with integer design variables x is subject to the following constraints:

- Manufacturing constraints:
  1. There must exist at least three plies along the whole length of the blade, which is simply assessed by the bound constraints:

$$1 \leqslant x_i \equiv m_i \leqslant 3, \quad x_{11+i} \equiv p_i = 10, \quad \text{for } i = 1,2,3. \tag{18}$$

  The remaining variables have the following box constraints:

$$0 \leqslant x_i \equiv m_i \leqslant 3, \quad x_{11+i} \equiv 1 \leqslant p_i \leqslant 10, \quad \text{for } i = 4,5,\dots,11. \tag{19}$$

  2. The maximum number of plies of the same material placed sequentially in any angle direction is limited to 3. Given the ply layout x, the stacking sequence is defined as $m_1,m_2,\dots$ excluding the plies with $m_i = 0$, from which can be determined the maximum number of plies of the same material, say $s_{\max}(x)$. Then, the following nonlinear, non-differentiable integer inequality constraint is prescribed:

$$c_1(x) = s_{\max}(x) - 3 \leq 0. \tag{20}$$

  This rule serves to reduce the transverse shear stress between plies and the free edge defects [23–25].
  The above manufacturing constraints were not taken into account in the design of the reference blade [12].
- Mechanical constraints:
  1. Maximum tip displacement constraint: usually, the tip displacement of the blade should not exceed a given value $u_{\max}$. With the aim of optimizing the blade previously designed [12], widely described in Section 2, let us assume $u_{\max} = 0.350$ m, which is the tip displacement for this reference blade. This is a nonlinear inequality constraint expressed as follows:

$$c_2(x) = u_{\text{tip}}(x) - u_{\max} \leqslant 0, \tag{21}$$

  where $u_{\text{tip}}(x)$ is the displacement of the tip of the blade whose ply layout is defined by x, determined from the IFEM analysis.
  2. Vibration frequency constraints: Wind turbine blades are flexible slender structures that are prone to vibrate and to interact with each other, especially when the main dynamic excitations take place predominantly in a similar range of frequencies compared to those corresponding to the lowest modes of the structure as a whole. Moreover, the design of blades is a stand-alone process, which may consider time-domain aeroelastic simulations for determining equivalent Ultimate Limit States (ULS) and Fatigue Limit States (FLS). These equivalent loads may not lead to a design, which is close to the optimal configuration for the nominal condition, in which the turbine is conceived to run most of the time. Therefore, the inclusion of ULS and FLS is not within the scope of this work. An essential aspect to be taken into account even during the design stage is to avoid the matching of natural frequencies and integer multiples of the angular speed of the rotor. This could be achieved by introducing constraints that can be directly derived from the Campbell diagram. The first one is a lower bound restriction given by

$$c_{\text{lower}}(x) = f_{\text{blade}} - (p + \alpha) f_{\text{rotor}} \geqslant 0, \tag{22}$$

  for $f_{\text{blade}} > p f_{\text{rotor}}$, and the second one is an upper bound restriction given by

$$c_{\text{upper}}(x) = (p - \alpha) f_{\text{rotor}} - f_{\text{blade}} \geqslant 0, \tag{23}$$

  for $p f_{\text{rotor}} > f_{\text{blade}}$, in which f_{blade} is a given natural frequency of the blade for the clamped-free boundary condition, f_{rotor} is the rotational frequency of the rotor, p is a multiple integer of the rotational frequency of the rotor. The later is also a positive safety factor, typically 0.05 or larger due to the fact that the natural frequency for the clamped-free boundary condition (for the structure attached to a rotating base) and the corresponding frequency considering the wind turbine as a whole that runs at nominal condition, are certainly different. Special attention must be paid to the fact that the blades suffer a stiffening due to the rotation and a stiffening or softening due to axial loads, which can be briefly described as:

$$K_g \propto \frac{\partial K_g}{\partial \Omega_1^2}\Omega_1^2 + \frac{\partial K_g}{\partial \Omega_2^2}\Omega_2^2 + \frac{\partial K_g}{\partial P_3}P_3, \tag{24}$$

  where K_g is the geometric part of the stiffness matrix, Ω_1 and Ω_2 are components of the angular velocity of the rotor lying on the plane normal to the axial direction of the blade, and P_3 is the component of actuating loads along the blade, see for instance [26,27]. For small and medium-sized wind turbines, the stiffening effect is very important and the corresponding Campbell diagram ought to be corrected to avoid designs that could result

in very conservative and therefore suboptimal solutions.
Given $f_{rotor} = 72\,\text{RPM} = 1.2\,\text{Hz}$, we prescribe the natural frequency of the blade to be separated ±5% from f_{rot} as well as from $3f_{rot}$ (the number of blades in the turbine being 3). This gives rise to the following nonlinear inequality constraints:

$$c_3(x) = 0.05f_{rot} - |f_{blade}(x) - f_{rot}| \geqslant 0, \tag{25}$$

$$c_4(x) = 0.05f_{rot} - |f_{blade}(x) - 3f_{rot}| \leqslant 0. \tag{26}$$

The value of $f_{blade}(x)$ is obtained as a result of the IFEM analysis of the blade whose ply layout is defined by x.

3. Maximum stress constraints: We use the maximum stress failure criterion [28–30] to verify the stresses in each ply of the blade, which is expressed by the following nonlinear and non-differentiable inequality constraints:

$$c_1^{(i)}(x) = -k\min(\sigma_1^{(i)}(x)) - X_C^{(i)} \leqslant 0, \tag{27}$$

$$c_2^{(i)}(x) = k\max(\sigma_1^{(i)}(x)) - X_T^{(i)} \leqslant 0, \tag{28}$$

$$c_3^{(i)}(x) = -k\min(\sigma_2^{(i)}(x)) - Y_C^{(i)} \leqslant 0, \tag{29}$$

$$c_4^{(i)}(x) = k\max(\sigma_2^{(i)}(x)) - Y_T^{(i)} \leqslant 0, \tag{30}$$

$$c_5^{(i)}(x) = -k\min(\tau_{12}^{(i)}(x)) - S_\tau^{(i)} \leqslant 0, \tag{31}$$

$$c_6^{(i)}(x) = k\max(\tau_{12}^{(i)}(x)) - S_\tau^{(i)} \leqslant 0, \tag{32}$$

applied to each non-empty ply i (having $m_i > 1$), where $X_T^{(i)}$ is the ultimate longitudinal tensile strength, $X_C^{(i)}$ is the ultimate longitudinal compressive strength, $Y_T^{(i)}$ is the ultimate transverse tensile strength, $Y_C^{(i)}$ is the ultimate transverse compressive strength, and $S_\tau^{(i)}$ is the ultimate shear strength, which are properties of the material m_i (see Table 2). Following [10], the material safety factor adopted is $k = 2.204$. $\sigma_1^{(i)}(x)$ and $\sigma_2^{(i)}(x)$ are the stresses in the material principal directions, and $\tau_{12}^{(i)}(x)$ is the maximal shear stress in ply i to be determined for each particular design x using IFEM. For an empty ply i, we force the above constraints to be automatically satisfied by setting $c_j^{(i)}(x) = 0$ ($j = 1,4,\ldots,6$) for $m_i = 0$.

3. Genetic algorithms

Given the integer nature of the design variables x and the non-differentiability of most of the constraints, meta-heuristic algorithms are most suitable for the solution of the optimization problem (15). Here, we use genetic algorithms (GA) [4], which are by far the most popular solvers for the optimal design of tapered laminates [5–7], including wind turbine blades [10,11].

Regarding to integer variables, Fagan et al. [11] used thirty-two integer variables to define the distribution of biaxial and triaxial layers in a structural design optimization of a composite wind turbine blade. Dal Monte et al. [8] proposed the use of integer variables to optimize the categorical variables of a multi-objective structural optimization problem of a HAWT composite blade, where each categorical variable represents the material, the orientation of the fibers with respect to the spanwise direction and thickness of the single layer. Here, the current implementation of GA is based on the algorithm proposed by Deep et al. [31], who introduced the Laplace crossover and the power mutation techniques to improve the performance of the GA solver in the presence of integer and mixed integer design variables. In this work, the implementation of this approach takes as platform the Distributed Evolutionary Algorithms in Python (DEAP) [32] as was proposed by Bre et al. [33] to optimize the categorical design variables of a residential building in order to improve its energy performance. Briefly, the steps for the current GA optimization process are summarized in the following pseudo-code:

```
population = random(popsize)
Fitness(population)
Update elite list
From 1 to #generations do
  offspring = Selection(population)
  offspring = Crossover(offspring)
  offspring = Mutation(offspring)
  Fitness(offspring)
  Update elite list
  population = offspring
End
```

The individuals of a population are ply layouts x satisfying the bound constraints. To be feasible, x must also satisfy the inequality constraints, Eqs. (20)–(26), (32). Following Deb [34], the inequality constraints are taken into account in the definition of the fitness function:

$$f(x) = \begin{cases} w(x) & \text{for feasible } x, \\ w(x_{worst}) + \sum_{j=1}^{4} \langle -c_j(x) \rangle + \sum j & \text{for unfeasible } x, \\ \quad = 1^6 \sum_{i=1}^{11} \langle -c_j^{(i)}(x) \rangle & \end{cases} \tag{33}$$

where x_{worst} is the individual which has the maximal weight among all the feasible individuals of a population, and $\langle y \rangle = (y + |y|)/2$ is the ramp function, so that a constraint penalizes the fitness only, if it is violated.

Note that at every fitness step, the mechanical constraints, Eqs. (21)–(26), (32), are obtained as results of IFEM analysis, making the current approach a simulation-based optimization method.

GA settings (population size, selection, crossover and mutation methods, the probability of mutation and crossover, etc.) depend on the characteristics of the optimization problem [35]. In this case, the best results were found for the GA configuration shown in Table 3.

3.1. Optimization procedure flowchart

In order to summarize the optimization procedure, Fig. 7 depicts the optimization flowchart. In each GA loop generation, the offspring population is obtained through the selection, crossover and mutation operation. During each fitness step, the objective $f_i(x)$, the mechanical and manufacture constraints are calculated for each individual x in the population.

Table 3
GA algorithm settings.

Parameter	Value
Number of individuals	48
Number of generations	100
Elite individuals	1
Selection	Tournament
Crossover method	Laplace
Crossover probability	100%
Mutation method	power
Mutation probability	0.5%

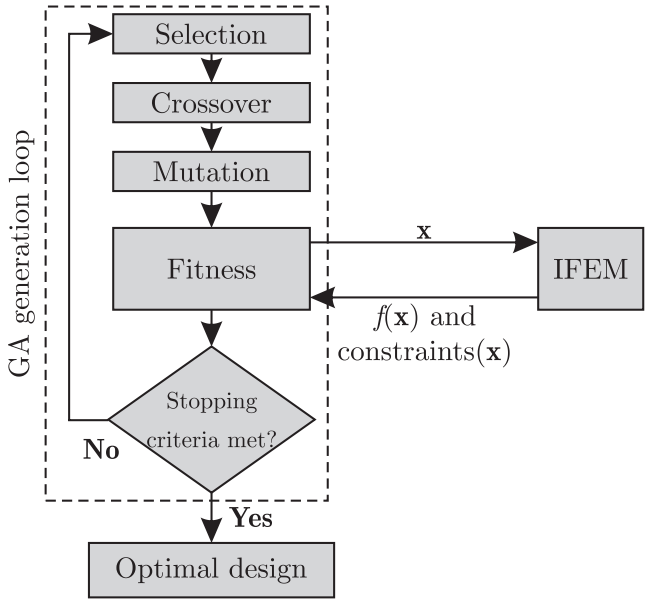

Fig. 7. Flowchart of the optimization procedure combining GA and IFEM.

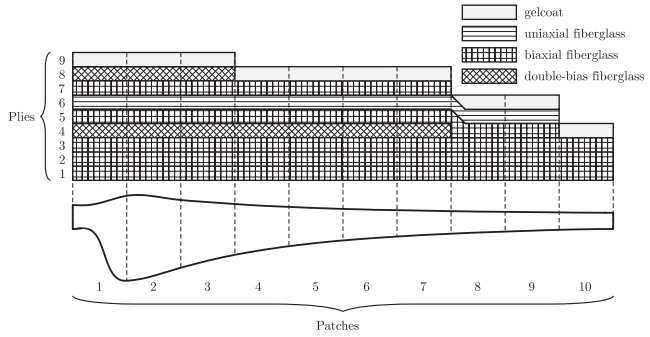

Fig. 8. Layout of the optimized blade. Empty plies (those with $m_i = 0$) have been discarded when numbering the plies, because they have zero thickness, and thus plies located above fall down to this position. For instance, in patch 8, since ply 4 does not exist ($m_4 = 0$), ply 5 becomes ply 4, forcing the ply above to fall by one position, i.e. ply 6 becomes ply 5.

Briefly, the new designs proposed by GA and given by the design variables are parameterized in a laminate definition indicating the material in each layer, and the extension of each layer along the blade. Once the laminate is defined, the stationary inertial forces around the rotation axis are computed considering the density and thickness of the composite, the turbine rotational velocity, and distance to the rotation axis. The total forces over the blade are computed by adding the nodal stationary inertial forces to the aerodynamic forces. These total forces are known data in the IFEM analysis.

Given the prescribed aerodynamic geometry and the total forces as known data, the IFEM solver is called. If it converges, this solution is subjected to a series of verification tests (detailed in Section 2.2), and if these tests are passed, the output is composed of the manufacturing shape of the wind turbine blade, the value of the objective function, and the value of the design constraints.

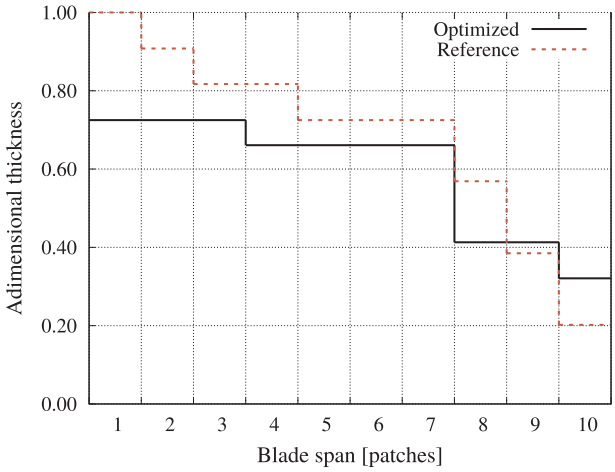

Fig. 10. Adimensional thickness of the shell skin for the reference and optimal designs.

The output of IFEM is fed to the GA algorithm for evaluation, and for the proposal of a new set of design candidates. This sequence is repeated until the convergence of the GA algorithm.

4. Results and discussion

Using GA as detailed in the previous section, we obtained the optimal layout of the current blade given by the vector of design variables

$$x_{\text{opt}} = [2\ \ 2\ \ 2\ \ 0\ \ 3\ \ 2\ \ 1\ \ 2\ \ 3\ \ 0\ \ 0\ \ |\ \ 10\ \ 10\ \ 10\ \ 8\ \ 7\ \ 9\ \ 9\ \ 8\ \ 3\ \ 4\ \ 1]. \tag{34}$$

Since $m_4 = m_{10} = m_{11} = 0$, plies 4, 10 and 11 actually do not exist. Henceforth, the laminate in the optimized blade has 8 plies (besides the outer gelcoat ply), following the stacking sequence (from the core): biaxial/biaxial/biaxial/double-bias/biaxial/uniaxial/biaxial/double-bias.

The optimal layout given by the design vector (34) is the one graphically represented in Fig. 8, where the empty plies (those with $m_i = 0$) have been discarded when numbering the plies, because these have zero thickness, and thus plies located above (towards the outside of the blade) fall down to this position. For instance, in patch 8, since ply 4 does not exist ($m_4 = 0$), ply 5 becomes ply 4. This forces all plies located above to fall by one position, i.e. ply 6 becomes ply 5. Hence, the resulting layout may have different but continuous stacking sequences, and in some patches, outer layers may be longer than the inner layers without losing continuity, see reference [7].

Fig. 9 depicts the thickness of the laminated composite material in the shell skin of the optimal blade design. Fig. 10 shows the comparison between the adimensional thickness of the shell skin for the reference and optimal wind turbine blade designs.

Regarding the weight of the blade that is the current objective function, the optimal blade weighs 24.28 kg, being 15.7% lighter than the reference blade (28.82 kg). It is important to remark that, because GA is a population based algorithm and due to the current parameterization permits the existence of two designs with the same weight and different distributions of the layup, it is possible that in the final population one may obtain two solution with these characteristic. We have not encountered that situation in this work. However, in such

Fig. 9. Thickness of the laminated composite material in the shell skin of the optimal design.

Table 4
Maximum and minimum principal stresses (σ_1 and σ_2) and shear stress τ_{12}, measured in [MPa]. All values are below 100 [MPa], ensuring that stresses remain in the linear elastic regime.

Ply	Material	maxσ_1	minσ_1	maxσ_2	minσ_2	maxτ_{12}	minτ_{12}
1	biaxial	93.23	−21.25	47.68	−47.01	28.67	−28.67
2	biaxial	76.69	−17.82	39.42	−41.60	25.90	−25.90
3	biaxial	62.67	−12.35	27.62	−36.48	24.51	−24.51
4	double-bias	52.28	−12.65	16.14	−34.29	23.40	−23.40
5	biaxial	53.12	−13.16	11.15	−39.66	28.98	−28.98
6	uniaxial	46.61	−4.31	4.04	−38.92	24.61	−24.61
7	biaxial	49.98	−19.72	20.76	−62.54	42.75	−42.75
8	double-bias	45.95	−23.83	25.98	−62.44	34.27	−34.27

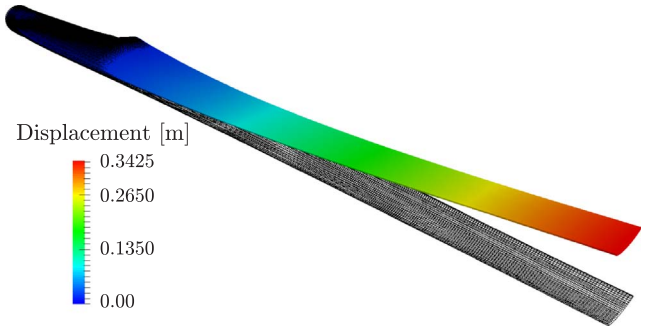

Fig. 11. Displacement modulus in the optimized blade. The prescribed aerodynamic geometry is plotted in wireframe. View from the leading edge.

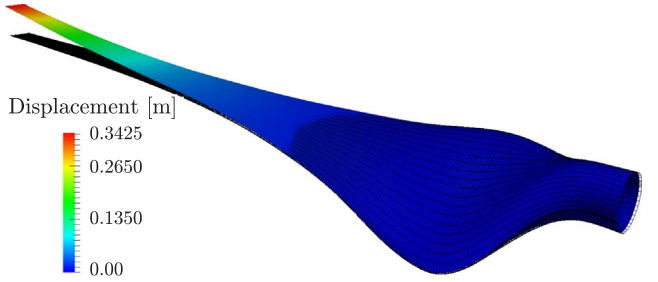

Fig. 12. Displacement modulus in the optimized blade. The prescribed aerodynamic geometry is plotted in wireframe. View from the trailing edge.

case, the final decision should be taken by the design engineer by considering other design aspects such as material cost, manufacturing complexity, and availability among others.

Besides satisfying all the manufacturing constraints, x_{opt} also satisfies all the mechanical constraints. Regarding the maximum stresses, this can be assessed by comparing those listed in Table 4 with their thresholds (dependent on the material of the ply) given in Table 2. Since the values of Table 4 are below 100 [MPa], all stresses remain in the linear elastic regime for a composite made of E-type glass fiber and epoxy resin [36,37].

Figs. 11 and 12 show the given efficient aerodynamic shape and the computed manufacturing shape. As it can be observed, the tip displacement in the optimized blade is $u_{tip} = 0.3425$ m, slightly smaller than that of the reference blade taken as the maximum admissible tip displacement $u_{max} = 0.350$ m in the inequality constraint (21).

Regarding vibrations, we consider the constraint first natural frequency of the optimal blade to be 4.456 Hz, quite far from both $f_{rot} = 1.2$ Hz the frequency of the rotor) and $3f_{rot} = 3.6$ Hz, preventing the occurrence of resonances in the operating conditions. Although they were not taken into account in the definition of the vibration constraints (25) and (26), the second and third natural frequencies are also

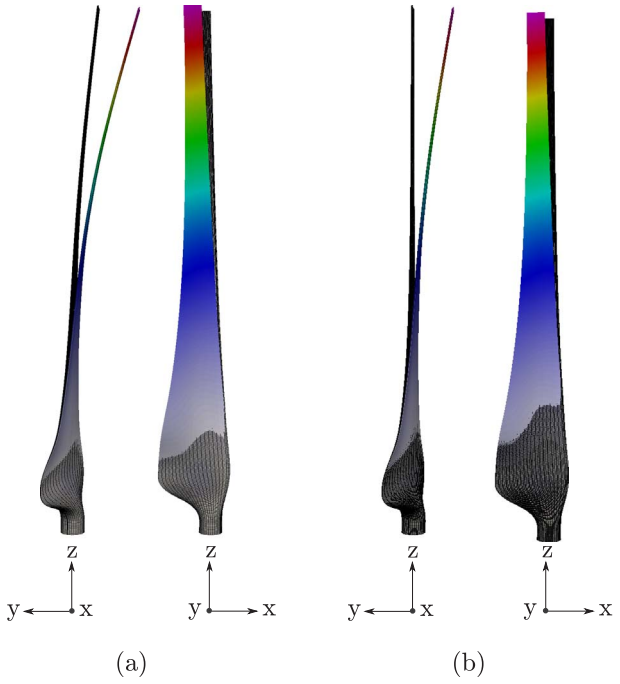

Fig. 13. First natural mode of vibration, flapwise predominant. a) depicted for the manufacturing shape of the blade, b) depicted for the loaded shape of the blade (represented by the color surface and amplified by a factor of 35).

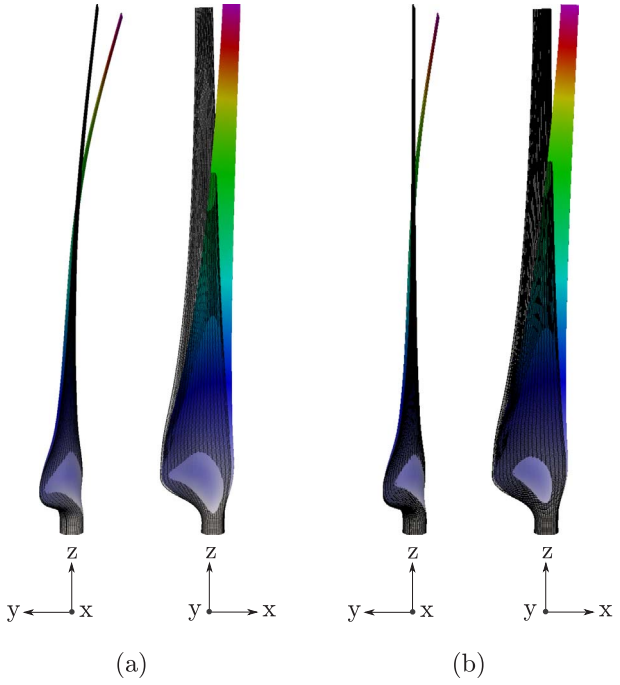

Fig. 14. Second natural mode of vibration, edgewise predominant. a) depicted for the manufacturing shape of the blade, b) depicted for the loaded shape of the blade (represented by the color surface and amplified by a factor of 35).

far from f_{rot} and $3f_{rot}$, reinforcing the safety margin of the blade. The first, second, and third natural vibration mode for the optimal blade are depicted in Figs. 13–15 respectively, for both the manufacturing and loaded shapes.

Finally, Table 5 compares the main characteristics of the optimal and the reference blades.

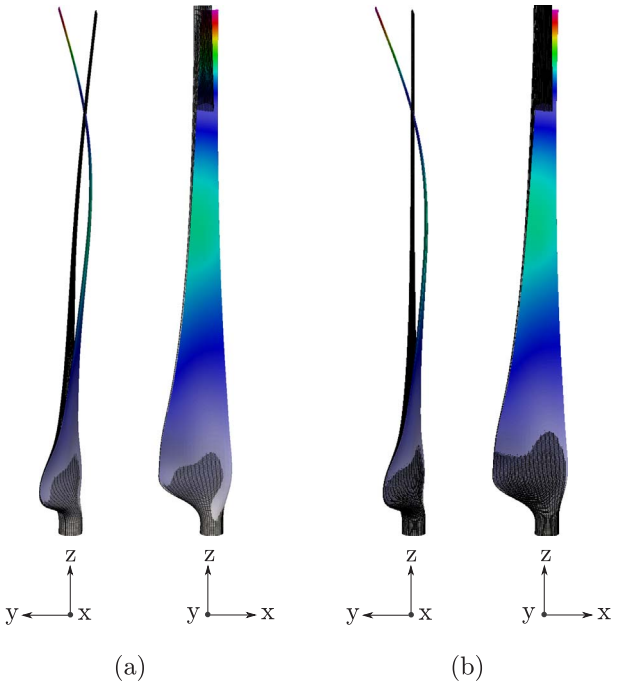

Fig. 15. Third natural mode of vibration, flapwise predominant. a) depicted for the manufacturing shape of the blade, b) depicted for the loaded shape of the blade (represented by the color surface and amplified by a factor of 35).

Table 5
Comparison between the reference and optimal blade designs.

Characteristic	Reference design	Optimal design
Blade weight	28.82 kg	24.28 kg
Tip deflection	0.350 m	0.3425 m
1st natural frequency	5.857 Hz	4.456 Hz
2nd natural frequency	9.935 Hz	8.012 Hz
3rd natural frequency	16.695 Hz	14.564 Hz

5. Conclusion

This work presents a new simulation-based optimization tool combining GA and IFEM for nonlinear shells for the simultaneous ply-order, ply-number and ply-drop optimization of the composite laminate for wind turbine blades. A unique feature of the IFEM structural solver is the computation of the manufacturing shape of the blade in such a way that it attains an efficient prescribed aerodynamic shape after large elastic deformations.

In the optimization procedure, the weight of the blade was minimized, subjected to mechanical (allowable tip deflection, maximum stress, natural vibration frequencies) and manufacturing constraints (maximum number of successive identical plies). The fiber continuity was assured by a proper definition of the design variables, avoiding impractical stacking solutions.

The application of the proposed methodology in an actual engineering case study demonstrated that this procedure is a robust redesign tool fully capable of accurately determining the optimal material stacking sequence of laminate wind turbine blades. Results showed weight reductions of up to 15% compared to a reference design, while satisfying all mechanical and manufacturing constraints.

Future work will be focused on the one hand, on multi-objective optimization considering the weight and stiffness of the laminated blade, and on the other hand, on the use of metamodel-based optimization to reduce optimization time.

Acknowledgments

The authors gratefully acknowledge the financial support from CONICET (Argentine Council for Scientific and Technical Research). A.E. Albanesi also acknowledges the National Technological University of Argentina (UTN) for Grants PID ENUTNFE0004405 and PID ASUTNFE0002425, and the National Agency of Scientific and Technological Promotion of Argentina (ANPCYT) for the Grant PICT 3396.

References

[1] Ghiasi H, Fayazbakhsh K, Pasini D, Lessard L. Optimum stacking sequence design of composite materials part II: Variable stiffness design. Compos Struct 2010;93:1–13.
[2] Ghiasi H, Pasini D, Lessard L. Optimum stacking sequence design of composite materials part I: constant stiffness design. Compos Struct 2009;90:1–11.
[3] Burton T, Jenkins N, Sharpe D, Bossanyi E. Wind Energy Handbook. 2nd ed. John Wiley and Sons; 2011.
[4] Goldberg DE, Holland JH. Genetic algorithms and machine learning. Mach Learn 1988;3(2):95–9.
[5] Kim J-S, Kim C-G, Hong C-S. Optimum design of composite structures with ply drop using genetic algorithm and expert system shell. Compos Struct 1999;46(2):171–87.
[6] Irisarri F-X, Lasseigne A, Leroy F-H, Le Riche R. Optimal design of laminated composite structures with ply drops using stacking sequence tables. Compos Struct 2014;107:559–69.
[7] Fan H-T, Wang H, Chen X-H. An optimization method for composite structures with ply-drops. Compos Struct 2016;136:650–61.
[8] Dal Monte A, Castelli MR, Benini E. Multi-objective structural optimization of a hawt composite blade. Compos Struct 2013;106:362–73.
[9] Dal Monte A, De Betta S, Castelli MR, Benini E. Proposal for a coupled aerodynamicstructural wind turbine blade optimization. Compos Struct 2017;159:144–56.
[10] Wang L, Kolios A, Nishino T, Delafin P-L, Bird T. Structural optimisation of vertical-axis wind turbine composite blades based on finite element analysis and genetic algorithm. Compos Struct 2016;153:123–38.
[11] Fagan EM, Flanagan M, Leen SB, Flanagan T, Doyle A, Goggins J. Physical experimental static testing and structural design optimisation for a composite wind turbine blade. Compos Struct 2017;164:90–103.
[12] Albanesi A, Fachinotti V, Peralta I, Storti B, Gebhardt C. Application of the inverse finite element method to design wind turbine blades. Compos Struct 2017;161:160–72.
[13] Fachinotti VD, Albanesi AE, Martinez Valle JM. Inverse finite element modeling of shells using the degenerate solid approach. Comput Struct 2015;157:89–98.
[14] Giguere PP, Selig MS. New airfoils for small horizontal axis wind turbines. ASME J Sol Energy Eng 1998;120(2):108–14.
[15] Berry D, Ashwill T. Design of 9-meter carbon-fiberglass prototype blades: Cx-100 and tx-100. Sandia National Laboratories Procedia Engineering Report SAND2007-0201; 2007. p. 1-46.
[16] Bir G, Migliore P. Preliminary structural design of composite blades for two- and three-bladed rotors. National Renewable Energy Laboratory (NREL) Report NREL/TP-500-31486; 2004. p. 1–37.
[17] Geuzaine C, Remacle J-F. Gmsh: a three-dimensional finite element mesh generator with built-in pre-and post-processing facilities. Int J Numer Meth Eng 2009;79(11):1309–31.
[18] Dvorkin EN, Bathe K-J. A continuum mechanics based four-node shell element for general nonlinear analysis. Eng Comput 1984;1:77–88.
[19] Simo JC, Fox DD, Rifai MS. On a stress resultant geometrically exact shell model. Part III: Computational aspects of the nonlinear theory. Comput Methods Appl Mech Eng 1990;79:21–70.
[20] Albanesi AE, Pucheta MA, Fachinotti VD. A new method to design compliant mechanisms based on the inverse beam finite element model. Mech Mach Theory 2013;65:14–28.
[21] Albanesi AE. Inverse design methods for compliant mechanisms [PhD thesis]. Faculty of Engineering and Water Sciences, National Littoral University, Santa Fe, Argentina; 2011.
[22] Eaton JW, Bateman D, Hauberg S, Wehbring R. GNU Octave version 4.0.3 manual: a high-level interactive language for numerical computations; 2016. URL:http://www.gnu.org/software/octave/doc/interpreter.
[23] Zein S, Madhavan V, Dumas D, Ravier L, Yague I. From stacking sequences to ply layouts: an algorithm to design manufacturable composite structures. Compos Struct 2016;141:32–8.
[24] Liu D, Toropov VV, Zhou M, Barton D, Querin O. Optimization of blended composite wing panels using smeared stiffness technique and lamination parameters. 51st AIAA/ASME/ASCE/AHS/ASC Structures, Structural Dynamics, and Materials Conference; 2010.
[25] Niu MCY. Airframe structural design. 2nd ed. Conmilit Press Ltd; 1999.
[26] Gebhardt CG, Roccia BA. Non-linear aeroelasticity: an approach to compute the response of three-blade large-scale horizontal-axis wind turbines. Renewable Energy 2014;66:495–514.
[27] Holm-Jorgensen K, Nielsen SRK. A component mode synthesis algorithm for multibody dynamics of wind turbines. J Sound Vibr 2009;326:753–67.
[28] Barbero EJ. Introduction to composite materials design. 2nd ed. CRC Press; 2011.

[29] Kaw AK. Mechanics of composite materials. 2nd ed. CRC Press; 2006.
[30] Jones R. Mechanics of composite materials. 2nd ed. Taylor and Francis; 1999.
[31] Deep K, Singh KP, Kansal ML, Mohan C. A real coded genetic algorithm for solving integer and mixed integer optimization problems. Appl Math Comput 2009;212(2):505–18.
[32] Fortin F-A, De Rainville F-M, Gardner M-A, Parizeau M, Gagn C. DEAP: evolutionary algo- rithms made easy. J Mach Learn Res July 2012;13:2171–5.
[33] Bre F, Silva AS, Ghisi E, Fachinotti VD. Residential building design optimisation using sensitivity analysis and genetic algorithm. Energy Build 2016;133:853–66.
[34] Deb K. An efficient constraint handling method for genetic algorithms. Comput Methods Appl Mech Eng 2000;18:311–38.
[35] Deb K. Multi-objective optimization using evolutionary algorithms vol. 16. John Wiley & Sons; 2001.
[36] Belingardi G, Paolino DS, Koricho EG. Investigation of influence of tab types on tensile strength of e-glass/epoxy fibereinforced composite materials. Proc Eng 2011;10:3279–84.
[37] Elanchezhian C, Vijaya Ramnath B, Hemalatha J. Mechanical behaviour of glass and carbon fibre reinforced composites at varying strain rates and temperatures. Proc Mater Sci 2014;6:1405–18.